THE JOURNAL OF BIOLOGICAL CHEMISTRY VOL. 287, NO. 1, pp. 159–169, January 2, 2012

Lipocalin-2 (24p3/Neutrophil Gelatinase-associated Lipocalin (NGAL)) Receptor Is Expressed in Distal Nephron and Mediates Protein Endocytosis*[S]

Received for publication, September 28, 2011, and in revised form, October 30, 2011 Published, JBC Papers in Press, November 14, 2011, DOI 10.1074/jbc.M111.308296

Christian Langelueddecke[‡], Eleni Roussa[§], Robert A. Fenton[¶1], Natascha A. Wolff[‡], Wing-Kee Lee[‡], and Frank Thévenod[‡2]

From the [‡]Institute of Physiology and Pathophysiology, Centre for Biomedical Training and Research (ZBAF), University of Witten/Herdecke, 58453 Witten, Germany, the [§]Institute of Anatomy and Cell Biology II, Albert-Ludwigs-Universität Freiburg, 79104 Freiburg, Germany, and the [¶]Department of Biomedicine, Aarhus University, DK-8000 Aarhus C, Denmark

Background: Localization and function of the lipocalin-2/NGAL/24p3 receptor (24p3R) in the kidney are unknown.
Results: 24p3R is expressed in apical plasma membranes of the distal nephron and mediates high-affinity protein endocytosis in renal cells.
Conclusion: 24p3R contributes to protein endocytosis and nephrotoxicity in distal nephron segments.
Significance: This is the first study to investigate localization and function of 24p3R in relevant epithelia.

In the kidney, bulk reabsorption of filtered proteins occurs in the proximal tubule via receptor-mediated endocytosis (RME) through the multiligand receptor complex megalin-cubilin. Other mechanisms and nephron sites for RME of proteins are unclear. Recently, the secreted protein 24p3 (lipocalin-2, neutrophil gelatinase-associated lipocalin (NGAL)), which is expressed in the distal nephron, has been identified as a sensitive biomarker of kidney damage. A high-affinity receptor for 24p3 (24p3R) that is involved in endocytotic iron delivery has also been cloned. We investigated the localization of 24p3R in rodent kidney and its role in RME of protein-metal complexes and albumin. Immunostaining of kidney tissue showed expression of 24p3R in apical membranes of distal tubules and collecting ducts, but not of proximal tubule. The differential expression of 24p3R in these nephron segments was confirmed in the respective cell lines. CHO cells transiently transfected with 24p3R or distal tubule cells internalized submicromolar concentrations of fluorescence-coupled proteins transferrin, albumin, or metallothionein (MT) as well as the toxic cadmium-MT (Cd^{2+}_7-MT) complex, which caused cell death. Uptake of MT or transferrin and Cd^{2+}_7-MT toxicity were prevented by picomolar concentrations of 24p3. An EC_{50} of 123 ± 50 nM was determined for binding of MT to 24p3R by microscale thermophoresis. Hence, 24p3R binds proteins filtered by the kidney with high affinity and may contribute to RME of proteins, including 24p3, and to Cd^{2+}_7-MT toxicity in distal nephron segments.

The kidney plays a major role in controlling physiological urinary protein excretion. Plasma proteins, which are filtered by the glomeruli, are efficiently reabsorbed by renal tubules so that less than 5% of filtered proteins are detected in the urine (1, 2). The majority of filtered proteins are reabsorbed in the PT[3] (3) by RME via the multiligand high-capacity receptor complex megalin-cubilin-amnionless (4, 5) and degraded in lysosomes (4). It is current dogma that neither the DT nor the collecting duct (CD) has specific features for RME, although both segments have the capability for protein endocytosis (6). In fact, several micropuncture studies indicated that distal parts of the nephron are able to reabsorb significant amounts of filtered proteins under physiological conditions (3, 7–12). However, the contribution of the DT to protein reabsorption varies depending on the nature of the proteins, their concentration, the tubular flow rate, and the experimental animal and ranges between 3 and 25% of filtered proteins (3, 7–12) but may further increase when the capacity for protein reabsorption in the PT is exceeded, as in the case of glomerular or PT damage (6, 13, 14).

A variety of noxious events can cause glomerular or PT damage, including infectious, immunologic, genetic, hypoxic, or toxic processes. For instance, exposure to toxic metals, such as cisplatinum or cadmium (Cd^{2+}), targets the PT to induce necrotic or apoptotic cell death (15, 16). Following chronic low-dose Cd^{2+} exposure, Cd^{2+} is complexed to the high-affinity metal-binding protein metallothionein (Cd^{2+}_7-MT), which is the major form of Cd^{2+} in the circulation (17). With a molecular mass of ~7 kDa, Cd^{2+}_7-MT is a low molecular weight protein complex, which is easily filtered by the glomeruli and reabsorbed via megalin-mediated RME by the PT (18, 19). Interestingly, there are indications that chronic Cd^{2+} nephro-

* This work was supported by Deutsche Forschungsgemeinschaft Grant TH345/11-1 and ZBAF (Centre for Biomedical Training and Research Witten/Herdecke University) (to F. T.).
[S] This article contains supplemental Figs. 1 and 2 and Table 1.
[1] Supported by the Lundbeck foundation and Danish Medical Research Foundation.
[2] To whom correspondence should be addressed: Institute of Physiology and Pathophysiology, ZBAF, University of Witten/Herdecke, Faculty of Health, Stockumer Str. 12, D-58453 Witten, Germany. Tel.: 49-2302-926221; Fax: 49-2302-926182; E-mail: frank.thevenod@uni-wh.de.

[3] The abbreviations used are: PT, proximal tubule; DCT, distal convoluted tubule; DT, distal tubule; 24p3R, receptor for 24p3; NGAL, neutrophil gelatinase-associated lipocalin; Cd^{2+}_7-MT, cadmium-MT; MT, metallothionein; CD, collecting duct; IMCD, inner medullary collecting duct; MTT, 3-(4,5-dimethylthiazol-2-yl)-2,5-diphenyltetrazolium bromide; PFA, paraformaldehyde; PM, plasma membrane(s); RME, receptor-mediated endocytosis; Tf, transferrin; CT, C-terminal: NT, N-terminal.

toxicity affects the DT as well, both in experimental animals (20) and in Cd^{2+}-exposed workers (21), although the mechanism of distal tubule damage has remained unresolved.

Recently, urinary neutrophil gelatinase-associated lipocalin (NGAL, rodent 24p3/human lipocalin-2) has emerged as a novel high-sensitivity biomarker of kidney damage that is upregulated by kidney injuries (22–25). NGAL binds iron through association with bacterial (26) as well as mammalian siderophores (27, 28), thereby affecting iron homeostasis of target cells and hence their survival and proliferation. During the course of renal insults, NGAL is secreted by the thick ascending limb of Henle loop, DT, and CD and excreted into the urine (25). It has been postulated that uptake of NGAL-siderophore-iron complexes by damaged nephron segments limits injury and promotes regeneration of damaged epithelia (29), but the underlying mechanisms are still unclear. Previously, Devireddy *et al.* (30) cloned a receptor for murine 24p3 whose affinity for 24p3/NGAL is almost 1000-fold higher (K_D ~92 pM) (31) than that of megalin (K_D ~60 nM) (32). The 24p3 receptor (24p3R) protein is expressed in the kidney and Madin-Darby canine kidney cells (30). Surprisingly, its localization and function in the nephron have not yet been investigated.

We have generated specific antibodies against rodent 24p3R and investigated its localization in rodent kidney as well as its function in transiently transfected Chinese hamster ovary (CHO) and renal DT cells. Here we demonstrate that 24p3R is expressed in the DT and medullary CD and is responsible for high-affinity RME of the low molecular weight protein MT as well as high molecular weight proteins, transferrin, and albumin in cultured cells. Furthermore, 24pR mediates $Cd^{2+}{}_7$-MT toxicity in cultured cells.

EXPERIMENTAL PROCEDURES

Materials—Metallothionein (rabbit apo-MT-1A or apo-MT-2) was from Bestenbalt LLC (Poska, Estonia) or IKZUS Proteomics (Genova, Italy). 24p3 was obtained from Enzo Life Sciences (Lörrach, Germany). Lipofectamine 2000 was from Invitrogen (Darmstadt, Germany). 3-(4,5-dimethylthiazol-2-yl)-2,5-diphenyl-tetrazolium bromide (MTT), paraformaldehyde (PFA), protease inhibitor mixture, and FITC-labeled bovine serum albumin were purchased from Sigma. Alexa Fluor 546-carboxylic acid succinimidyl ester and Alexa Fluor 546-transferrin (Tf) from human serum were from Molecular Probes Europe BV (Invitrogen).

Antibodies—Polyclonal antibodies were generated in rabbits against the rat peptide sequence for 24p3R (GenBank™ accession number NP_803156.2). The epitope sequences for 24p3R COOH-terminal (α-CT-24p3R) and NH_2-terminal (α-NT-24p3R) antibodies were CDHVPLLATPNPAL and GALPPNASGWEQPPNSC, respectively. Rabbits were immunized thrice intracutaneously, and after final bleeding, antibodies were purified by Sepharose affinity purification (HPLC profile and mass spectrometry with minimum 80% purity) by ImmunoGlobe GmbH (Himmelstadt, Germany). Both epitopes selected show 100% identity in mouse (GenBank accession number Q9D9E0) and rat 24p3R. Preimmune serum and antigenic peptide preabsorption experiments confirmed antibody specificity (supplemental Fig. 1). Commercially available antibodies were used at the following dilutions: α1-subunit of Na^+,K^+-ATPase (Cell Signaling Technology; 1:500), cathepsin L clone 33/2 (Abcam; 1:150), calbindin (Swant; 1:2500). Secondary antibodies were as follows. Horseradish peroxidase (HRP)-anti-rabbit IgG (GE Healthcare Europe GmbH, Munich, Germany) was used for immunoblotting and diluted 1:1000 to 1:5000; Alexa Fluor 488-conjugated anti-rabbit IgG and Alexa Fluor 633-conjugated anti-mouse IgG (Molecular Probes), FITC-conjugated anti-mouse IgG (Jackson ImmunoResearch Laboratories, Suffolk, UK), HRP-conjugated anti-rabbit IgG (DAKO, Hamburg, Germany), and indocarbocyanine (Cy3)-coupled anti-rabbit IgG (Jackson ImmunoResearch Laboratories) were used for immunostaining.

Immunofluorescence and Peroxidase Light Microscopy of Mouse Kidney—Experiments on mice were carried out in strict accordance with state health and ethical regulations. Care of animals was in accordance with institutional guidelines. The protocol for sacrifice of animals was approved by the Committee on the Ethics of Animal Experiments of the University of Freiburg (permit number X-07/27A). C57/BL6 male adult mice were anesthetized with ketamine (90 mg/kg of body weight) and xylazine (12 mg/kg of body weight) and fixed with 4% PFA by perfusion through the heart. Kidneys were excised, postfixed in 4% PFA overnight at 4 °C, dehydrated, and embedded in paraffin. Staining was performed as described previously (33) Sections were incubated with α-CT-24p3R (1 μg/ml) and with Cy3 (1:600) or HRP (1:50) anti-rabbit IgG. For double immunofluorescence, fixed α-CT-24p3R was incubated together with anti-calbindin antibody. Sections were viewed with a Zeiss Axioplan2 fluorescence microscope with ApoTome module (Jena, Germany). Control experiments were performed by substituting the primary antibody with preimmune serum (supplemental Fig. 1*A*).

Immunohistochemistry of Rat Kidney—Animal housing conditions and experiments on male Wistar rats (Taconic Europe) were approved by the Danish Ministry of Justice. All procedures have been described in detail previously (34). α-CT-24p3R was used at 0.25 μg/ml. For preincubation experiments, affinity-purified antibodies were preincubated at 4 °C overnight with 10-fold molar excess of antigenic peptide. Images were taken using an HCX PL APO 63 oil objective lens on a Leica DMRE microscope (Leica Microsystems, Herlev, Denmark).

Cell Culture—CHO-K1 (Chinese hamster ovary; < passage 40) cells were provided by Dr. H. Koepsell (University of Würzburg) and cultured in F12 medium supplemented with 10% fetal bovine serum and 100 μg/ml penicillin/streptomycin. Immortalized mouse distal convoluted tubule cells (mDCT209; < passage 40) were a gift from Dr. P.A. Friedman (University of Pittsburgh) (35). Immortalized WKPT-0293 Cl.2 cells (< passage 70) isolated from the S1 segment of rat PT were cultured as described previously (36). Unless otherwise indicated, cells were grown for 48 h prior to experiments.

Transient Transfections—The full-length clone of rat 24p3R (GenBank accession number NM_177421.3) (IRAKp961A-13231Q, I.M.A.G.E. clone 7312276) was obtained from imaGenes (Berlin, Germany) and cloned into the expression vector pcDNA3.1+ carrying neomycin (G418) and ampicillin resistance (Invitrogen). CHO cells were transiently transfected 24 after seed-

ing using Lipofectamine 2000 in medium without antibiotics. After 6 h, medium was replaced, and cells were incubated for an additional 48 h. For isolation of plasma membranes, transfected cells were transferred to 75-cm^2 flasks 48 h after transfection. 24p3R-positive cells (24p3R-CHO) were selected in 500 μg/ml G418 supplemented medium for 2 weeks with medium change every 48 h.

Reverse Transcription-Polymerase Chain Reaction (RT-PCR)—cDNA was synthesized from 2 μg of total RNA, and RT-PCR was carried out with Maxima^{TM} Hot Start Green PCR master mix (Fermentas). Primers, cycling protocols, GenBank accession numbers, and product sizes are shown in supplemental Table 1.

Isolation of Plasma Membranes—Plasma membranes were obtained by differential ultracentrifugation at 4 °C. Cells were homogenized by nitrogen pressure cavitation in a Parr Instruments 45-ml cell disruption vessel (Moline, IL) for 2 min at 350 p.s.i. To remove unbroken cells, nuclei, and large debris, homogenate was centrifuged at 300 × *g* for 10 min. Mitochondria were pelleted at 4000 × *g* for 10 min, and the resulting supernatant was centrifuged for 30 min at 35,000 × *g* to yield a microsomal fraction in the pellet. Plasma membranes were isolated by discontinuous sucrose gradient ultracentrifugation exactly as described previously (37). The plasma membrane fraction was washed with 10× volume of 5 mM Tris/HCl, pH 7.4, centrifuged for 30 min at 233,000 × *g*, and resuspended in 5 mM Tris/HCl, pH 7.4, supplemented with protease inhibitor mixture. Plasma membrane enrichment was verified by immunoblotting and showed about 20-fold enrichment of Na^+,K^+-ATPase (data not shown).

Immunoblotting—Cells were lysed by sonication (Branson Sonifier S-250D, Danbury, CT), and protein concentration was determined by Bradford assay (38). Equal protein (0.5–5 μg) was subjected to 7.5% SDS-PAGE and immunoblotted, as described previously (39). Signals were quantified using ImageJ or TINA 2.09 software.

Cell Viability Assay—$Cd^{2+}{}_7$-MT was prepared from rabbit apo-MT (19), and cell viability was determined by the MTT test (36), both as described previously.

Immunofluorescence Microscopy of Cultured Cells—In most experiments, cells were fixed, permeabilized, stained, and imaged as described previously (39). Briefly, cells were fixed with 4% PFA and permeabilized with 1% SDS. MT was coupled to Alexa Fluor 546, as reported previously (40). Primary α-CT-24p3R and α-NT-24p3R antibodies were used at 5 μg/ml, and secondary Cy3 or Alexa Fluor 488 anti-rabbit IgG was diluted 1:600. Where indicated, confocal microscopy using a TCS SP5 confocal laser scanning microscope (Leica, Wetzlar, Germany) was performed essentially as described previously (40).

Live Immunofluorescence Staining of Cultured Cells—Experiments with non-permeabilized cells (see Fig. 3, *B* and *D*) were performed as described elsewhere (41) with the following modifications. Cells were blocked for 1 h with 1% bovine serum albumin and incubated with 5 μg/ml α-NT-24p3R for 2 h followed by Alexa Fluor 488-conjugated secondary antibody (1:600) for 1 h before fixation with 4% PFA at room temperature for 30 min.

Quantification of 24p3R-mediated Internalization of Fluorescent Dye-labeled Proteins—MT was coupled to Alexa Fluor 546, as described previously (40). Concentration dependence of uptake of Alexa Fluor 546-coupled MT, Alexa Fluor 546-Tf, and FITC-albumin was estimated following a 24-h incubation period in serum-free medium. In addition, time-dependent uptake of 1.4 μM Alexa Fluor 546-coupled MT was determined after 6–36 h in serum-free medium. For each experiment, 10 images of transfected and non-transfected cells were acquired and quantified as described earlier (39) or by counting the percentage of transfected cells with internalized fluorescent dye-labeled proteins (positive cells). To determine 24p3R-specific uptake of fluorescent dye-labeled proteins, fluorescence values in the vector-transfected cells were subtracted from the fluorescence values in the corresponding 24p3R-transfected cells.

Microscale Thermophoresis—Binding interactions between 24p3R-CHO plasma membrane vesicles and the ligand Alexa Fluor 546-MT were measured using microscale thermophoresis, which determines differences in the thermophoretic properties of single molecules or ligands and ligand-receptor complexes in microliter volumes on a Monolith NT.015 (NanoTemper Technologies GmbH, Munich, Germany). Thermophoresis is based on the thermodiffusive properties of biomolecules in liquids (42–44). Binding of a fluorescent ligand to its receptor changes the hydration shell of the receptor and thereby its entropy. An infrared (IR) laser diode creates a hot spot, which induces movement of the complex along the temperature gradient and depends on the concentration of the ligand-receptor complex. For each plasma membrane preparation, specific binding of Alexa Fluor 546-MT (0.7 μM) to 24p3R membrane vesicles was compared with nonspecific binding to vector membrane vesicles by serial vesicle dilutions in 5 mM Tris/HCl, pH 7.4. The vesicle concentration showing the greatest "signal-to-noise" ratio was used for determining EC_{50} values. Briefly, a titration series with constant 24p3R and varying ligand Alexa Fluor 546-MT was preincubated for 30 min at 37 °C in the dark to achieve ligand-receptor binding equilibrium. All measurements were performed in hydrophobic capillaries at room temperature. Plotting normalized fluorescence F_{norm} at a given time *t* against the Alexa Fluor 546-MT concentration resulted in a binding curve, and EC_{50} values were obtained from fitting the binding curves with the Hill equation assuming a Hill coefficient of 1.0.

Statistics—Unless otherwise indicated, the experiments were repeated at least three times. Analyses by unpaired Student's *t* test or for more than two groups, one-way analysis of variance assuming equality of variance with Levene's test, and Tukey's post hoc test were carried out with GraphPad Prism 5.0. Results with $p < 0.05$ were considered to be statistically significant.

RESULTS

24p3R Is Expressed Apically in Rodent DCT and IMCD Cells—The 24p3R has been previously found by immunoblotting to be expressed in mouse kidney tissue and Madin-Darby canine kidney cells, a DT cell line (30). Using the specific antibody against the C-terminal sequence of 24p3R (α-CT-24p3R),

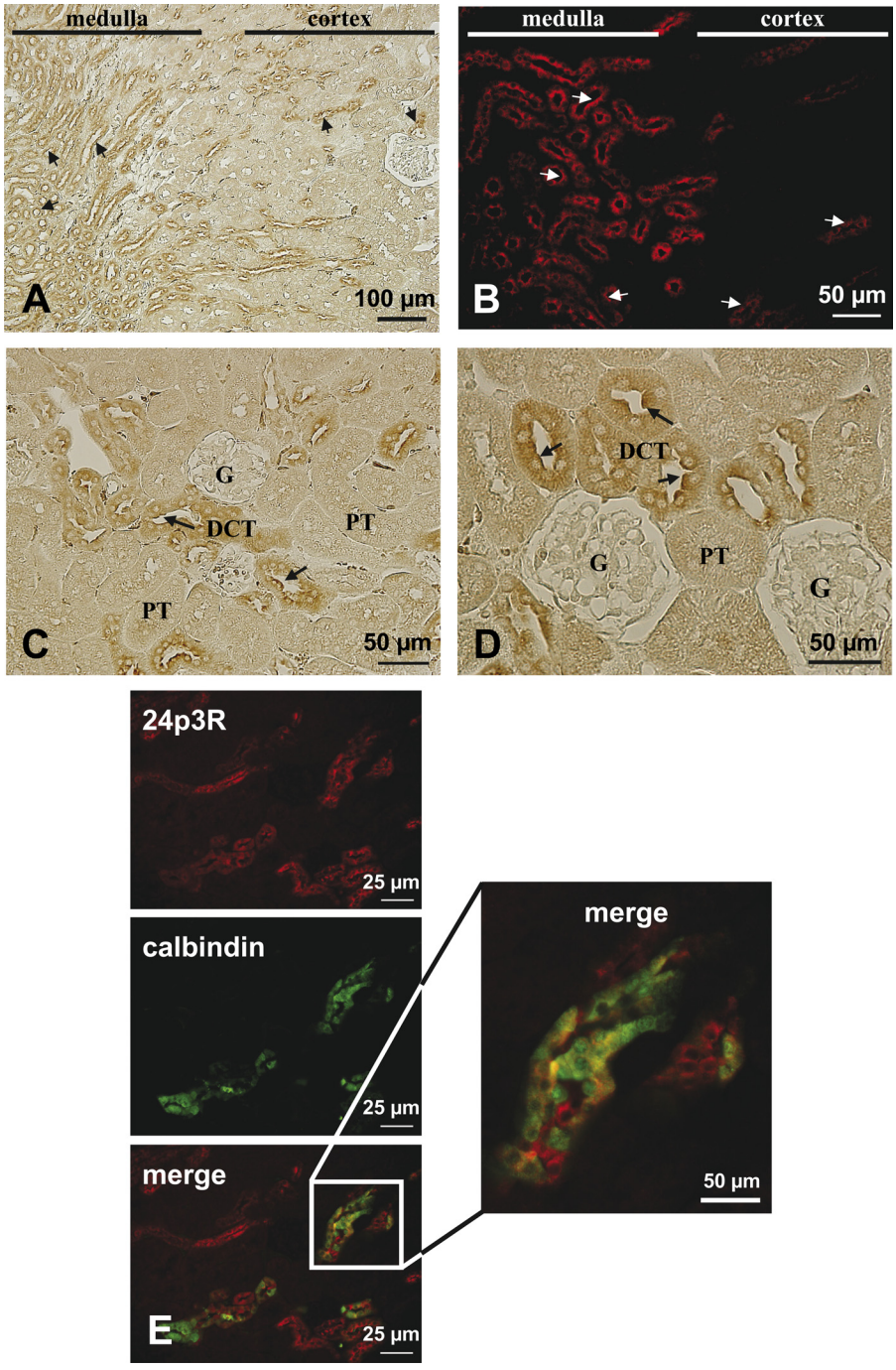

FIGURE 1. **Cellular distribution of 24p3R in murine kidney by immunoperoxidase (*A*, *C*, and *D*) and immunofluorescence (*B* and *E*) microscopy.** *A*, 24p3R immunolabeling with α-CT-24p3R is observed at the apical membrane (*arrows*) of distinct tubular segments in both renal cortex and medulla. *B*, labeling pattern of 24p3R in murine renal cortex and medulla shows strong luminal localization (*arrows*) of the protein. *C*, in the renal cortex, cells resembling the DCT are positive for 24p3R (*arrows*), but not renal PT and glomeruli (*G*). *D*, higher magnification of an area in murine renal cortex showing prominent apical 24p3R labeling (*arrows*) in most cells of the DCT but not in the PT and glomeruli. *E*, double immunofluorescence labeling for 24p3R (*red*) and calbindin (*green*) in murine renal cortex shows co-localization of the proteins in several cells, indicating expression of 24p3R in the DCT and connecting tubules.

immunolabeling was present in both renal cortex and medulla in mouse kidney (Fig. 1, *A* and *B*). Medullary outer stripe and medullary CD revealed strong 24p3R immunostaining, which appeared sharp and partly localized to apical cell membranes. In renal cortex, prominent 24p3R apical and intracellular immunostaining was observed in the distal convoluted tubules (DCT) (Fig. 1, *C* and *D*, *arrows*). In contrast, in glomeruli and PT 24p3R, expression was not detectable. Double labeling for 24p3R and calbindin, a marker for late DCT and connecting tubule (calbindin is expressed in some cortical collecting duct cells in the rat, but its abundance is drastically reduced when compared with late DCT and connecting tubule) (45, 46), showed a complex cellular labeling pattern (Fig. 1*E*).The majority of DCT cells demonstrated co-localization of the two proteins, 24p3R apically and calbindin intracellularly. Other cells, however, were 24p3R-positive but calbindin-negative, suggest-

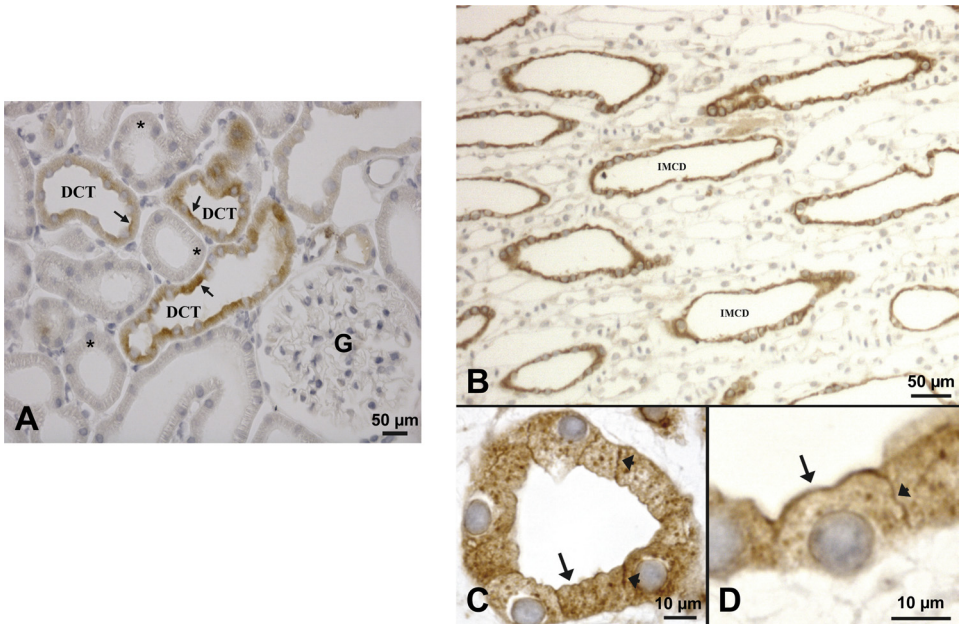

FIGURE 2. **Immunohistochemical localization of 24p3R in the rat kidney.** *A*, in the renal cortex, using α-CT-24p3R 24p3R localizes to tubules that morphologically resemble the DCT. Diffuse staining of the DCT cells is observed, but some labeling is associated with the apical plasma membrane (*arrows*). PT are not labeled (*asterisks*). *G* = glomerulus. *B*, 24p3R is detected throughout the IMCD. *C* and *D*, at higher magnification, 24p3R labeling is clearly associated with both the apical (*arrows*) and the lateral cell membrane (*arrowheads*).

ing that 24p3R is expressed in both early and late DCT. When sections were incubated with preimmune serum, a diffuse, weak, nonspecific labeling throughout the renal tissue could be observed, demonstrating specificity of the labeling obtained with α-CT-24p3R (supplemental Fig. 1*A*).

In rat kidney, 24p3R was also predominantly expressed in the DCT cells, both apically (Fig. 2*A*, *arrows*) and intracellularly (Fig. 2*A*). Glomeruli and other cortical tubular segments (including PT) were not stained (Fig. 2*A*, *asterisks*). Another location of strong 24p3R expression was inner medullary collecting ducts (IMCD) (Fig. 2, *B–D*). At higher magnification, 24p3R was clearly localized luminally (Fig. 2, *C* and *D*, *arrows*) and laterally (Fig. 2, *C* and *D*, *arrowheads*). Intracellular punctate 24p3R staining was also detected (Fig. 2, *C* and *D*), suggesting intracellular vesicles. No staining was observed after preabsorption of the peptide with the immunizing peptide (not shown). Overall, the distribution of 24p3R was comparable in mouse and rat kidney. Similar results were obtained with α-NT-24p3R, although the antibody showed more nonspecific background.

24p3R Is Expressed in the Rodent Distal Tubule Cell Line mDCT209—The expression of 24p3R was further investigated in immortalized DCT (mDCT209 (35)) and PT (WKPT-0293 Cl.2 (36)) cell lines. As shown in Fig. 3*A*, strong staining of 24p3R was detected with the specific antibody against the NH_2-terminal sequence of 24p3R (α-NT-24p3R) in mDCT209 cells by laser scanning confocal microscopy, which extended to cellular borders, whereas no major staining was detected in WKPT-0293 Cl.2. This is in agreement with the distribution of 24p3R in the corresponding nephron segments in rodent kidneys (Figs. 1 and 2). Plasma membrane localization of 24p3R in mDCT209 cells was confirmed by live staining with α-NT-24p3R using non-permeabilized cells (Fig. 3*B*, *upper panel*, *arrows*). Both rat and murine full-length cDNAs of 24p3R contain a single open reading frame of 520 amino acids (30), and an ~60-kDa polypeptide should be detected. No signal was detectable for 24p3R in both homogenate and plasma membranes (PM) of WKPT-0293 Cl.2 cells (Fig. 3*B*). In contrast, a double band at ~60 kDa was clearly detectable in PM of mDCT209 cells (Fig. 3*B*, *lower panels*, *arrows*), but not in homogenate, indicating an enrichment of 24p3R. Furthermore, when α-CT-24p3R was preabsorbed with a 10-fold excess of the antigenic peptide, the double band at ~60 kDa vanished, confirming specificity of the signal (Fig. 3*B*). An additional signal at ~140 kDa was also detected in mDCT209 cells, which disappeared by co-incubation with antigenic peptide (Fig. 3*B*) and could represent a 24p3R dimer. These data were complemented by RT-PCR for 24p3R in mDCT209 cells, which yielded only one band (Fig. 3*C*).

24p3R Mediates Endocytosis of MT, Tf, and Albumin in 24p3R-CHO and mDCT209 Cells—In contrast to HEK293 cells in which expressed 24p3R was trapped intracellularly (supplemental Figs. 1*B* and 2),[4] CHO cells expressed 24p3R in the PM, thus allowing study of putative functions of the receptor. Transient transfection of 24p3R induced overexpression of the gene product (Fig. 3, *D–F*, supplemental Fig. 1*C*) that could be detected in the PM using both α-NT-24p3R (Fig. 3*D*, *arrows*) and α-CT-24p3R (Fig. 3*E*, supplemental Fig. 1*D*, *arrows*). Moreover, live staining of non-permeabilized cells clearly demonstrated surface staining of 24p3R using α-NT-24p3R (Fig. 3*D*, *arrowheads*).

Next we investigated the internalization of the filtered low molecular weight protein MT as well as of the high molecular weight proteins albumin and Tf, which are all ligands of the megalin-cubilin-amnionless complex in the PT ((18, 19); reviewed in Refs. 4–6). 24p3R- and vector-CHO cells were exposed to 0.35–2.8 μM Alexa Fluor 546-MT, Alexa Fluor

[4] C. Langelueddecke and F. Thévenod, unpublished results.

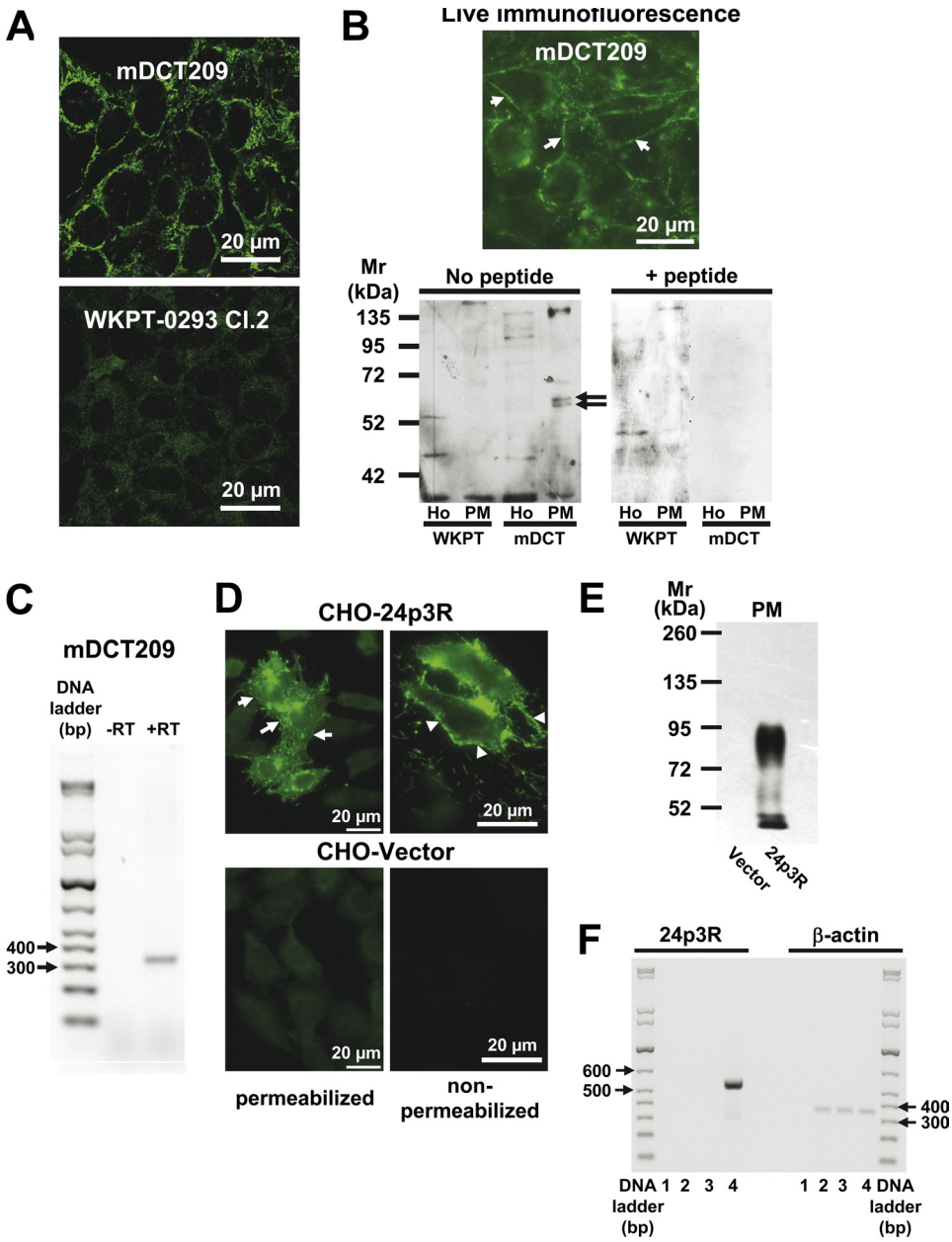

FIGURE 3. *A–C*, 24p3R is expressed in a distal convoluted tubule (mDCT209) but not in a proximal tubule (WKPT-0293 Cl. 2) cell line. *A*, laser scanning confocal immunofluorescence micrographs reveal 24p3R using α-NT-24p3R in plasma membranes and intracellular compartments of mDCT209, but not in WKPT-0293 Cl.2 cells. *B*, immunoblots of homogenates (*Ho*) and the PM are performed in the absence or after preabsorption of α-CT-24p3R with 10-fold excess of antigenic peptide. A specific double band at ~60 kDa (*arrows*) is detected in the PM of mDCT209 cells only (*lower panels*) in accordance with live immunofluorescence staining of mDCT209 cells (*upper panel*). *C*, a PCR product of 332 bp is amplified from mDCT209 cDNA using specific primers for murine 24p3R (+*RT*), but not from the control reaction without reverse transcriptase (−*RT*). *D–F*, CHO cells transiently express rat 24p3R. *D*, immunofluorescence microscopy with α-NT-24p3R reveals 24p3R in plasma membranes (*arrows*) and intracellular compartments of 24p3R-CHO cells only. Live immunofluorescence staining of non-permeabilized cells confirms surface expression of 24p3R (*arrowheads*). *E*, immunoblotting of the PM with α-CT-24p3R show strong immunoreactive signals in 24p3R-CHO cells only. *F*, in 24p3R-CHO cells, a PCR product of 540 bp is amplified (*lane 4*). *Lane 1*, no template; *lane 2*, no transfection; *lane 3*, vector transfection. The housekeeping gene β-actin is used as a control.

546-Tf, or FITC-albumin for 24 h. The magnitude of ligand uptake in 24p3R-transfected cells was about 2–3-fold that of vector-transfected cells and showed high-affinity saturating at ~1 μM of the ligand with the exception of MT, which showed the greatest magnitude of uptake (Fig. 4, *A* and *B*). Furthermore, co-localization of internalized Alexa Fluor 546-MT (1.4 μM for 18 h) with the lysosomal marker cathepsin-L was demonstrated in 24p3R-CHO cells, thus proving 24p3R-mediated endocytosis and subsequent trafficking to lysosomes (Fig. 4*C*). Similarly, Alexa Fluor 546-MT (2.8 μM for 24 h) was internalized by mDCT209 cells, which express 24p3R (Fig. 4*D*).

24p3R Mediates $Cd^{2+}{}_7$-MT Toxicity in 24p3R-CHO and mDCT209 Cells—In previous studies (39, 47), we demonstrated that in PT cells, the divalent metal transporter DMT1 is expressed in lysosomal membranes where it mediates efflux of Cd^{2+} from endocytosed $Cd^{2+}{}_7$-MT into the cytosol and subsequent mitochondrial apoptosis (reviewed in Refs. 48 and 49).

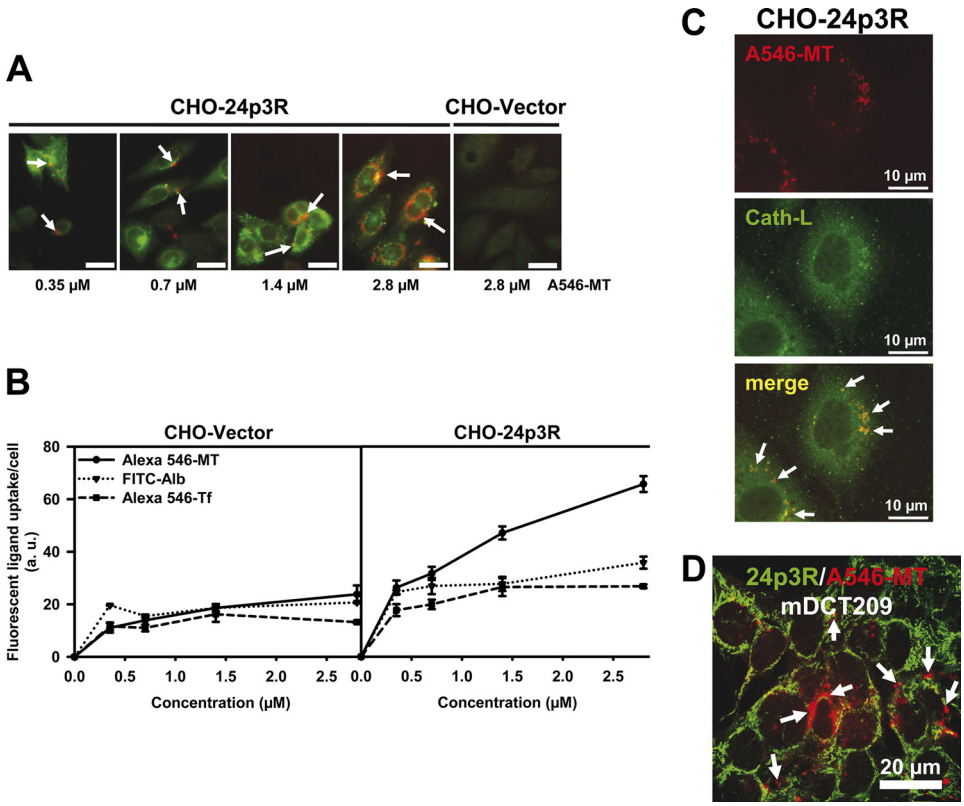

FIGURE 4. *A–C*, 24p3R mediates endocytosis of metallothionein, transferrin, and albumin in 24p3R-CHO cells. *A*, 24p3R-CHO cells, but not vector-CHO cells, internalize Alexa Fluor 546-metallothionein (*A546-MT*) (*arrows*) for 24 h, which is concentration-dependent. *Scale bar* = 30 μm. *B*, the graph demonstrates concentration-dependent internalization of Alexa Fluor 546-MT, Alexa Fluor 546-Tf, and FITC-albumin (*FITC-Alb*) in vector- and 24p3R-CHO cells after 24 h. Means ± S.E. of 3–6 different experiments are plotted. *C*, confocal images of internalized Alexa Fluor 546-MT and the lysosomal marker cathepsin L (*Cath-L*) in 24p3R-CHO cells show co-localization of both proteins (*arrows*). *D*, confocal images of endogenous 24p3R (*green*) and Alexa Fluor 546-MT (2.8 μM for 24 h) show internalization of Alexa Fluor 546-MT in mDCT209 cells (*arrows*).

Here we tested whether this mechanism is also operative in 24p3R-CHO cells as another approach to monitor the function of 24p3R. Hence, we measured cell viability with and without $Cd^{2+}{}_7$-MT as an "end point" of 24p3R-mediated RME. As shown in Fig. 5*A*, cell viability, as measured by MTT assay, significantly decreased as a function of the $Cd^{2+}{}_7$-MT concentration (up to 2.8 μM MT saturated by 20 μM Cd^{2+} for 24 h), which clearly mirrored the concentration dependence of Alexa Fluor 546-MT internalization (Fig. 5*A*). A similar relationship between cell viability and Alexa Fluor 546-MT internalization was observed in the kinetics of a fixed $Cd^{2+}{}_7$-MT concentration (1.4 μM MT and 9.8 μM Cd^{2+}) for 0–36 h (Fig. 5*B*). Similarly, mDCT209 cells, which express 24p3R, showed a concentration-dependent decrease of cell viability induced by $Cd^{2+}{}_7$-MT (Fig. 5*C*).

To prove that both Alexa Fluor 546-MT internalization and $Cd^{2+}{}_7$-MT cell death were caused by 24p3R in 24p3R-CHO cells, MT binding was competed with a saturating concentration of 500 pM 24p3 (K_D for 24p3R ~92 pM (31)). As shown in Fig. 5, *D* and *E*, 500 pM 24p3 largely prevented Alexa Fluor 546-MT (0.7 μM) uptake and $Cd^{2+}{}_7$-MT (0.7 μM) toxicity when compared with no difference in vector-CHO cells (data not shown). This experiment was repeated with Alexa Fluor 546-Tf (0.7 μM) and also confirmed 24p3R-mediated uptake of Tf that could be abolished by co-incubation with 500 pM 24p3 (Fig. 5*F*) (comparable results were obtained with 2.8 μM Alexa Fluor 546-Tf; data not shown). Similar results were also obtained in mDCT209 cells where Alexa Fluor 546-MT (0.7 μM for 24 h) internalization and $Cd^{2+}{}_7$-MT toxicity (0.35 μM MT/2.45 μM Cd^{2+} for 24 h) were significantly reduced (but not abolished, possibly due to concomitant 24p3R-independent endocytosis) by co-incubation with 500 pM 24p3 (Fig. 5, *G* and *H*).

24p3R Binds Alexa Fluor 546-MT with High Affinity—Direct Alexa Fluor 546-MT binding to 24p3R was quantified by microscale thermophoresis (42–44). For each transfection experiment, specific binding of Alexa Fluor 546-MT to 24p3R-CHO PM vesicles was compared with unspecific binding to vesicles from vector-CHO cells (Fig. 6*A*). In fact, the thermophoretic signal of the Alexa Fluor 546-MT-24p3R complex linearly depended on the 24p3R expression level (Fig. 6*B*). A typical thermophoresis experiment with constant 24p3R-CHO PM and varying Alexa Fluor 546-MT ligand concentration (20 nM-10 μM) is shown in Fig. 6*C*. In three different experiments, an EC_{50} of 123 ± 50 nM was determined (mean ± S.D.).

DISCUSSION

We investigated the distribution of 24p3R in rodent kidney, which was identically distributed in mouse and rat kidney (Figs. 1 and 2). In the cortex, it was mainly found in the DCT, but not in the PT (Figs. 1, *C–E*, and 2*A*), and in the medulla, strong levels of expression were detected in IMCD (Figs. 1, *A* and *B*, and 2, *B–D*), both intracellularly and in plasma membranes. This differential 24p3R expression was also observed in cell lines derived from proximal and distal

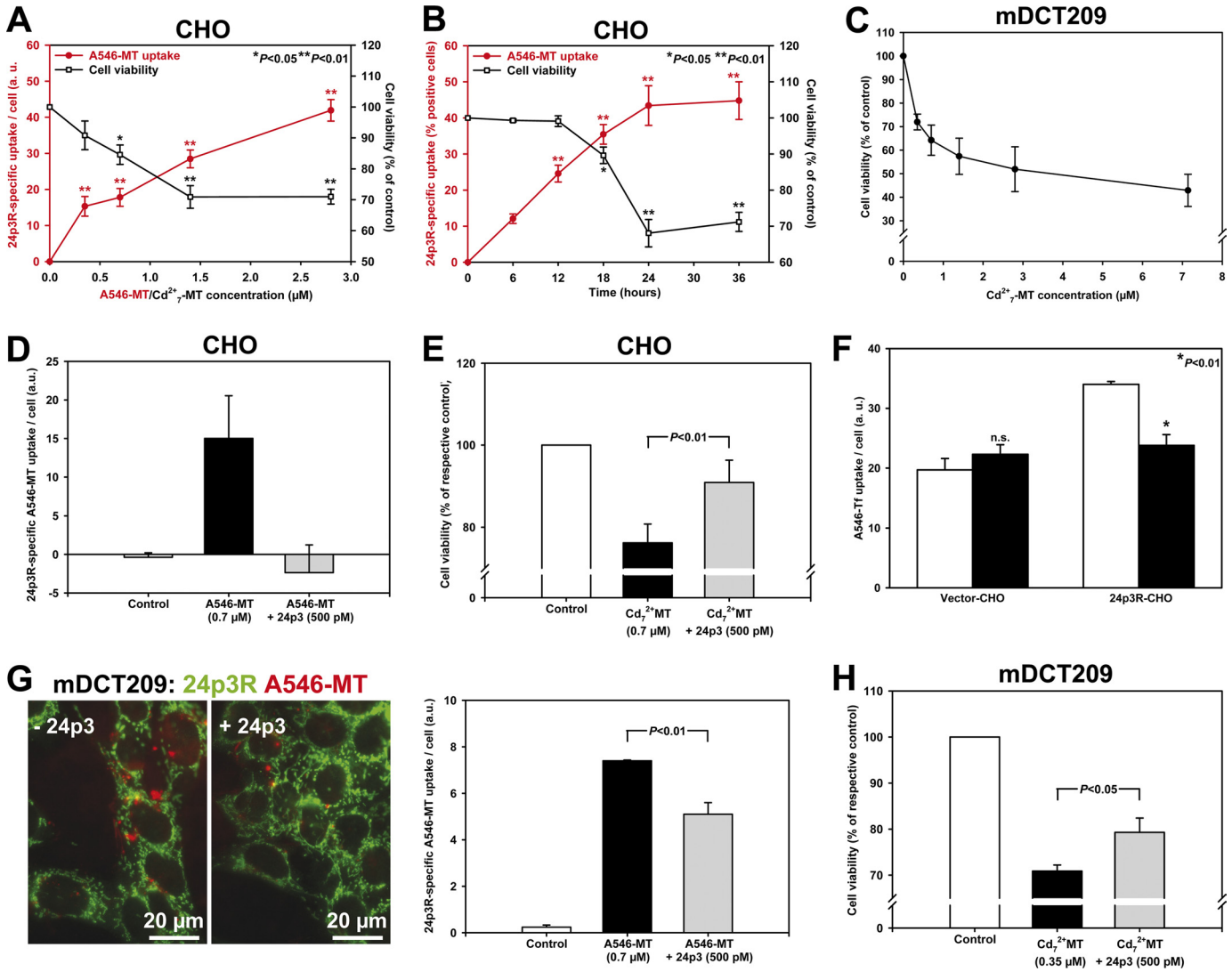

FIGURE 5. **24p3R mediates Cd^{2+}_7-MT toxicity in 24p3R-CHO cells and mDCT209 cells, which is rescued by 24p3.** *A*, in 24p3R-CHO cells, concentration-dependent Alexa Fluor 546-MT uptake (*a.u.* = arbitrary fluorescence units) after 24 h (as in Fig. 4*B*) mirrors concentration-dependent toxicity of Cd^{2+}_7-MT after 24 h by MTT assay. Means ± S.E. of 3–8 experiments are shown. Cell viability of vector-CHO cells was similar to untreated controls (90.2 ± 4.6% with 2.8 μM Cd^{2+}_7-MT; $n = 4$). *B*, kinetics of Alexa Fluor 546-MT (1.4 μM) uptake and Cd^{2+}_7-MT (10 μM Cd^{2+} and 1.4 μM MT) toxicity correlate in 24p3R-CHO cells. Means ± S.E. of 3–4 experiments are shown. Cell death of vector-CHO cells at 36 h is comparable with untreated controls (98.7 ± 2.1% with 1.4 μM Cd^{2+}_7-MT; $n = 4$; not significant). *C*, concentration-dependent toxicity of mDCT209 cells after 24 h of exposure to Cd^{2+}_7-MT determined by MTT assay. Means ± S.E. of 3 experiments are shown. *D*, 24p3 prevents Alexa Fluor 546-MT internalization. Means ± S.E. of 5 different images with 160–200 cells per experimental condition are shown. *E*, 24p3 abolishes the decrease of cell viability induced by Cd^{2+}_7-MT (5 μM Cd^{2+} and 0.7 μM MT). Means ± S.E. of 4 experiments are plotted. *F*, transient transfection of CHO cells with 24p3R increases Alexa Fluor 546-Tf (0.7 μM) internalization ~2-fold, which is abolished by 500 pM 24p3. Means ± S.E. of 5 different images with 170–250 cells per experimental condition are shown. *n.s.* = not significant. *G*, 24p3 competes with Alexa Fluor 546-MT internalization in mDCT209 cells, which indicates that Alexa Fluor 546-MT endocytosis is mediated by 24p3R (fluorescent images). Means ± S.E. of 5 different images with 180–200 cells per experimental condition are shown in the *right panel*. *H*, 24p3 rescues the decrease of cell viability induced by Cd^{2+}_7-MT (2.45 μM Cd^{2+} and 0.35 μM MT). Means ± S.E. of 4–5 experiments are plotted. Statistical analysis using one-way analysis of variance compares experimental conditions with and without 24p3. 24p3 alone was 99.6 ± 1.9% of non-treated controls (not shown).

nephron segments (Fig. 3). Interestingly, 24p3R expression was also detected in primary cultures of rat collecting duct cells.[5]

Besides its established function as a receptor for lipocalin-2/NGAL/24p3 (30, 31), a putative role of 24p3R in RME of (metal-binding) proteins was tested with a focus on the putative ligands MT, Tf, and albumin based on the following rationale. (i) These proteins bind metals, such as iron, zinc, or cadmium, but also calcium (17, 50–52); (ii) they are filtered by the kidney glomeruli (17, 53); and (iii) they are ligands of the megalin-cubilin-amnionless receptor complex in the PT (4).

In CHO cells overexpressing 24p3R, the magnitude of uptake of all three proteins was increased by maximally 2–3-fold (Fig. 4*B*). Putative ligands were internalized at sub- to low micromolar concentrations (Fig. 4*B*), indicating high-affinity binding to the receptor. From microscale thermophoresis experiments, an EC_{50} of MT binding to 24p3R was calculated to 123 ± 50 nM, which indicates a >500-fold higher affinity than its affinity to the megalin receptor (18). Moreover, uptake of MT and Tf was competed by picomolar concentrations of 24p3 (Fig. 5, *D*, *F*, and

[5] B. Edemir, C. Langelueddecke, and F. Thévenod, unpublished results.

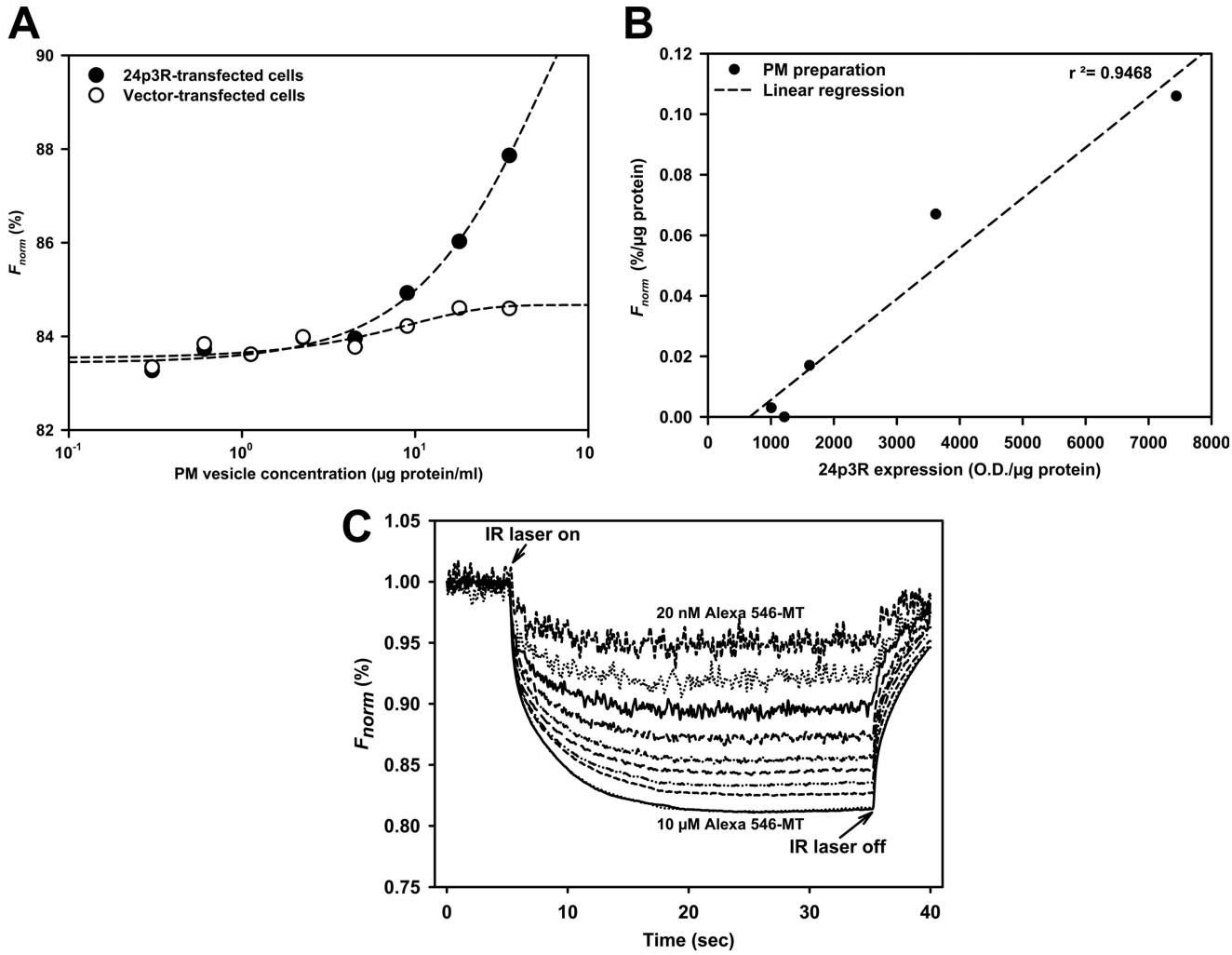

FIGURE 6. **Alexa Fluor 546-MT binding to plasma membrane vesicles of rat 24p3R-CHO cells using microscale thermophoresis.** *A*, the normalized fluorescence (F_{norm}) of bound Alexa Fluor 546-MT (0.7 μM) is higher in PM vesicles isolated from 24p3R-CHO when compared with vector-CHO cells. *B*, the normalized fluorescence (F_{norm}) of bound Alexa Fluor 546-MT (0.7 μM) correlates with the expression of 24p3R in transfected CHO cells, as determined by immunoblotting. *O.D.*, optical density. *C*, the analytical curves at 20 nM–10 μM Alexa Fluor 546-MT display four phases: the baseline (homogeneous distribution of fluorescent ligand and ligand-receptor complex), the temperature jump after applying the IR laser beam (movement of unbound ligand, which is a very rapid process), the thermophoresis (movement of ligand-receptor complexes, which usually lasts ~30 s), and the re-equilibration of all reagents after switching off the laser (with two components, a rapid one for the unbound ligand and a slow phase due to back diffusion of complexes). The IR laser is switched on at $t = 5$ s, the fluorescence decreases as the temperature increases, and the labeled MT moves away from the heated spot because of thermophoresis. When the IR laser is switched off, the molecules diffuse back. The thermophoretic depletion of unbound Alexa Fluor 546-MT is about four times that of Alexa Fluor 546-MT bound to 24p3R.

G), demonstrating high-affinity binding of 24p3 to its receptor and proving specificity of binding. The significant uptake of all three proteins in vector-transfected CHO cells indicates that additional uptake pathways are present in CHO cells (*e.g.* Tf receptor or fluid-phase endocytosis), and this could also account for the incomplete block of Alexa Fluor 546-MT uptake and $Cd^{2+}{}_7$-MT toxicity by 500 pM 24p3 in mDCT209 cells (Fig. 5, *G* and *H*). Using embryonic collecting duct or Madin-Darby canine kidney cells, Yang *et al.* (54) demonstrated that iron bound to Tf or 24p3 is taken up by two independent pathways with no overlapping specificity. This work, which assumes mutually exclusive uptake mechanisms of Tf and 24p3 in renal cells, apparently contradicts our observations of 24p3R-specific Tf binding and endocytosis in CHO cells that is prevented by 500 pM 24p3 (Fig. 5*F*). The work of Yang *et al.* (54) showed fluorescent images of Alexa Flour 488-Tf uptake in the presence of 24p3. Unfortunately, uptake of Alexa Fluor 488-Tf in the absence of 24p3 was not shown, and quantitative analysis of Alexa Fluor 488-Tf uptake was not performed, which would have been helpful to distinguish between 24p3R- and Tf receptor-mediated Tf uptake. Here we carried out quantitative analysis of the fluorescence data to clarify the competition of Tf uptake by 24p3 in vector- and 24p3R-transfected CHO cells (Figs. 4*B* and 5). The observed Tf uptake in the presence of 24p3 in the study by Yang *et al.* (54) and in our study most likely represents uptake via a Tf receptor (55). Assuming a K_D of Tf for the Tf receptor of about 5 nM (56) and a K_D of Tf for the 24p3R in the same magnitude as the EC_{50} of metallothionein (~100 nM), a significant proportion of Tf should be taken up by 24p3R in the concentration range tested (0.35–2.8 μM Tf).

Moreover, proteins internalized via 24p3R were trafficked to lysosomes, as shown for MT (Fig. 4*C*), suggesting lysosomal degradation of endocytosed proteins. This is important because this observation is in line with the data by Yang *et al.* (54), who

showed co-localization of endocytosed 24p3 in renal cells with acidic intracellular compartments expressing DMT1. We (39, 47) and others (57) have previously demonstrated expression of DMT1 in lysosomes of PT cells and hepatocytes. Therefore we used the property of MT as a high-affinity Cd^{2+}-binding protein to further characterize RME via 24p3R. In PT cells, endocytosed $Cd^{2+}{}_7$-MT is degraded in lysosomes and free Cd^{2+} transported via DMT-1 into the cytosol, which induces cell death (39, 58). Indeed, a similar mechanism was operative in 24p3R-transfected CHO cells and mDCT209 cells and $Cd^{2+}{}_7$-MT-induced cell death could be prevented by co-incubation with 24p3 (Fig. 5, *E* and *H*). Overall, these data strongly support the notion that the whole machinery for RME of proteins via 24p3R is present in the distal nephron where it may operate under certain physiological and pathophysiological circumstances.

Although bulk protein reabsorption takes place in the PT, experimental evidence has demonstrated that a small but significant proportion of filtered proteins is reabsorbed by the distal nephron (3, 7–12). Considering that megalin-cubilin-amnionless operates as a high-capacity, low-affinity receptor complex for endocytotic reabsorption of filtered proteins (4, 6), a certain proportion of these proteins should bypass reabsorption in the PT, either as the consequence of low affinity (*e.g.* MT with a K_D of ~100 μM (18)) or due to exhaustion of the reabsorptive capacity of the system (*e.g.* following glomerular or PT damage and ensuing proteinuria) (6, 13, 14, 53). A high-affinity protein reabsorption system in the distal nephron, as suggested by the present study, could contribute to exhaustive protein reabsorption by the nephron under physiological conditions, as deduced from previous micropuncture studies, or limit protein losses associated with renal diseases, including various forms of inherited or acquired Fanconi syndrome (53).

Chronic cadmium toxicity targets the kidney PT (48), largely due to RME of filtered $Cd^{2+}{}_7$-MT via megalin (18, 19). However, other segments of the nephron are also affected, although the literature on the subject is scarce (20, 21). It is conceivable that some filtered MT/$Cd^{2+}{}_7$-MT escapes PT reabsorption and reaches distal nephron segments (see above). MT is excreted into the urine of both non-exposed and cadmium-exposed humans (for a review, see Ref. 17). In cadmium-exposed humans, urinary MT originates from the damaged PT epithelium. However, in non-exposed healthy individuals, this indicates that filtered MT indeed escapes PT reabsorption (59). Accordingly, Sabolic *et al.* (17) observed MT droplets in the PT lumen of adult rats, which vanished in the distal nephron, suggesting reabsorption in these nephron segments.

Lipocalin-2/NGAL/24p3 plays a role as an iron-sequestering protein in the antibacterial innate immune response (60), and lipocalin-2-deficient mice have increased susceptibility to bacterial infections in the urinary tract (24). In this process, 24p3R in the distal nephron is thought to mediate iron sequestration into epithelia and thereby promote bacteriostasis. Hence, the predominant localization of 24p3R in IMCD could participate in a line of defense against ascending infections and is compatible with the described function of 24p3 in bacteriostasis (29). In addition, lipocalin-2/NGAL/24p3 is induced by distal nephron segments and released into the urine following renal damage, suggesting its involvement in autocrine/paracrine modulation of renal epithelial defense and repair (25, 29). Other postulated non-antibacterial functions of 24p3 include regulation of cell proliferation (61) or apoptosis (62) in the context of pathological conditions. However, the presence of a receptor for 24p3 in distal nephron segments suggests additional unknown functions of 24p3R and its endogenous ligand(s) in the kidney, such as adaptive response to cell stress and anti-apoptosis, which are the aim of ongoing studies.

Acknowledgments—We thank Dr. H. Koepsell (Institute of Anatomy and Cell Biology, University of Würzburg, Germany) for CHO-K1 (Chinese hamster ovary) cells, Dr. P. A. Friedman (Department of Pharmacology and Chemical Biology, University of Pittsburgh School of Medicine, Pittsburgh, PA) for mDCT209 cells, Dr. U. Hopfer (Department of Physiology and Biophysics, Case Western Reserve University, Cleveland, OH) for WKPT-0293 Cl.2 cells, Dr. M. Reinhard (ImmunoGlobe GmbH) for advice for generation and use of the antibodies, and Drs. S. Duhr and M. Jerabek-Willemsen (NanoTemper Technologies GmbH) for advice about the use of microscale thermophoresis.

REFERENCES

1. Boylan, J. W. (1979) *Kidney Int.* **16,** 247–250
2. Maack, T., Park, C. H., and Camargo, M. J. (1992) in *The Kidney: Physiology and Pathophysiology* (Seldin, D. W., and Giebisch, G., eds), pp. 3005–3038, Raven Press, New York
3. Tojo, A., and Endou, H. (1992) *Am. J. Physiol.* **263,** F601–F606
4. Christensen, E. I., Verroust, P. J., and Nielsen, R. (2009) *Pflugers Arch.* **458,** 1039–1048
5. Christensen, E. I., and Birn, H. (2002) *Nat. Rev. Mol. Cell Biol.* **3,** 256–266
6. Nielsen, R., and Christensen, E. I. (2010) *Pediatr. Nephrol.* **25,** 813–822
7. Straus, W. (1964) *J. Histochem. Cytochem.* **12,** 470–480
8. Cortney, M. A., Sawin, L. L., and Weiss, D. D. (1970) *J. Clin. Invest.* **49,** 1–4
9. Leber, P. D., and Marsh, D. J. (1970) *Am. J. Physiol.* **219,** 358–363
10. Roy, A. K., and Raber, D. L. (1972) *J. Histochem. Cytochem.* **20,** 89–96
11. Galaske, R. G., Van Liew, J. B., and Feld, L. G. (1979) *Kidney Int.* **16,** 394–403
12. Madsen, K. M., Harris, R. H., and Tisher, C. C. (1982) *Kidney Int.* **21,** 354–361
13. Birn, H., and Christensen, E. I. (2006) *Kidney Int.* **69,** 440–449
14. Kastner, C., Pohl, M., Sendeski, M., Stange, G., Wagner, C. A., Jensen, B., Patzak, A., Bachmann, S., and Theilig, F. (2009) *Am. J. Physiol. Renal Physiol.* **296,** F902-F911
15. Pabla, N., and Dong, Z. (2008) *Kidney Int.* **73,** 994–1007
16. Johri, N., Jacquillet, G., and Unwin, R. (2010) *Biometals* **23,** 783–792
17. Sabolic, I., Breljak, D., Skarica, M., and Herak-Kramberger, C. M. (2010) *Biometals* **23,** 897–926
18. Klassen, R. B., Crenshaw, K., Kozyraki, R., Verroust, P. J., Tio, L., Atrian, S., Allen, P. L., and Hammond, T. G. (2004) *Am. J. Physiol. Renal Physiol.* **287,** F393–F403
19. Wolff, N. A., Abouhamed, M., Verroust, P. J., and Thévenod, F. (2006) *J. Pharmacol. Exp. Ther.* **318,** 782–791
20. Girolami, J. P., Bascands, J. L., Pécher, C., Cabos, G., Moatti, J. P., Mercier, J. F., Haguenoer, J. M., and Manuel, Y. (1989) *Toxicology* **55,** 117–129
21. Lauwerys, R., and Bernard, A. (1989) *Toxicol. Lett.* **46,** 13–29
22. Mori, K., Lee, H. T., Rapoport, D., Drexler, I. R., Foster, K., Yang, J., Schmidt-Ott, K. M., Chen, X., Li, J. Y., Weiss, S., Mishra, J., Cheema, F. H., Markowitz, G., Suganami, T., Sawai, K., Mukoyama, M., Kunis, C., D'Agati, V., Devarajan, P., and Barasch, J. (2005) *J. Clin. Invest.* **115,** 610–621
23. Mishra, J., Ma, Q., Prada, A., Mitsnefes, M., Zahedi, K., Yang, J., Barasch, J., and Devarajan, P. (2003) *J. Am. Soc. Nephrol.* **14,** 2534–2543
24. Berger, T., Togawa, A., Duncan, G. S., Elia, A. J., You-Ten, A., Wakeham,

A., Fong, H. E., Cheung, C. C., and Mak, T. W. (2006) *Proc. Natl. Acad. Sci. U.S.A.* **103,** 1834–1839
25. Paragas, N., Qiu, A., Zhang, Q., Samstein, B., Deng, S. X., Schmidt-Ott, K. M., Viltard, M., Yu, W., Forster, C. S., Gong, G., Liu, Y., Kulkarni, R., Mori, K., Kalandadze, A., Ratner, A. J., Devarajan, P., Landry, D. W., D'Agati, V., Lin, C. S., and Barasch, J. (2011) *Nat. Med.* **17,** 216–222
26. Goetz, D. H., Holmes, M. A., Borregaard, N., Bluhm, M. E., Raymond, K. N., and Strong, R. K. (2002) *Mol. Cell* **10,** 1033–1043
27. Devireddy, L. R., Hart, D. O., Goetz, D. H., and Green, M. R. (2010) *Cell* **141,** 1006–1017
28. Bao, G., Clifton, M., Hoette, T. M., Mori, K., Deng, S. X., Qiu, A., Viltard, M., Williams, D., Paragas, N., Leete, T., Kulkarni, R., Li, X., Lee, B., Kalandadze, A., Ratner, A. J., Pizarro, J. C., Schmidt-Ott, K. M., Landry, D. W., Raymond, K. N., Strong, R. K., and Barasch, J. (2010) *Nat. Chem. Biol.* **6,** 602–609
29. Schmidt-Ott, K. M., Mori, K., Li, J. Y., Kalandadze, A., Cohen, D. J., Devarajan, P., and Barasch, J. (2007) *J. Am. Soc. Nephrol.* **18,** 407–413
30. Devireddy, L. R., Gazin, C., Zhu, X., and Green, M. R. (2005) *Cell* **123,** 1293–1305
31. Devireddy, L. R., Teodoro, J. G., Richard, F. A., and Green, M. R. (2001) *Science* **293,** 829–834
32. Hvidberg, V., Jacobsen, C., Strong, R. K., Cowland, J. B., Moestrup, S. K., and Borregaard, N. (2005) *FEBS Lett.* **579,** 773–777
33. Brandes, A., Oehlke, O., Schümann, A., Heidrich, S., Thévenod, F., and Roussa, E. (2007) *Am. J. Physiol. Regul. Integr Comp. Physiol.* **293,** R2400-R2411
34. Moeller, H. B., Knepper, M. A., and Fenton, R. A. (2009) *Kidney Int.* **75,** 295–303
35. Gesek, F. A., and Friedman, P. A. (1992) *J. Clin. Invest.* **90,** 429–438
36. Lee, W. K., Torchalski, B., Kohistani, N., and Thévenod, F. (2011) *Toxicol. Sci.* **121,** 343–356
37. Thévenod, F., and Schulz, I. (1988) *Am. J. Physiol.* **255,** G429–G440
38. Bradford, M. M. (1976) *Anal. Biochem.* **72,** 248–254
39. Abouhamed, M., Wolff, N. A., Lee, W. K., Smith, C. P., and Thévenod, F. (2007) *Am. J. Physiol. Renal Physiol.* **293,** F705–F712
40. Wolff, N. A., Lee, W. K., and Thévenod, F. (2011) *Toxicol. Lett.* **203,** 210–218
41. Wolff, N. A., Liu, W., Fenton, R. A., Lee, W. K., Thévenod, F., and Smith, C. P. (2011) *J. Cell Mol. Med.* **15,** 209–219
42. Duhr, S., and Braun, D. (2006) *Proc. Natl. Acad. Sci. U.S.A.* **103,** 19678–19682
43. Wienken, C. J., Baaske, P., Rothbauer, U., Braun, D., and Duhr, S. (2010) *Nat. Commun.* **1,** 100
44. Baaske, P., Wienken, C. J., Reineck, P., Duhr, S., and Braun, D. (2010) *Angew. Chem. Int. Ed. Engl.* **49,** 2238–2241
45. Loffing, J., Loffing-Cueni, D., Valderrabano, V., Kläusli, L., Hebert, S. C., Rossier, B. C., Hoenderop, J. G., Bindels, R. J., and Kaissling, B. (2001) *Am. J. Physiol. Renal Physiol.* **281,** F1021–F1027
46. Câmpean, V., Kricke, J., Ellison, D., Luft, F. C., and Bachmann, S. (2001) *Am. J. Physiol. Renal Physiol.* **281,** F1028–F1035
47. Abouhamed, M., Gburek, J., Liu, W., Torchalski, B., Wilhelm, A., Wolff, N. A., Christensen, E. I., Thévenod, F., and Smith, C. P. (2006) *Am. J. Physiol. Renal Physiol.* **290,** F1525-F1533
48. Thévenod, F. (2003) *Nephron. Physiol.* **93,** 87–93
49. Thévenod, F. (2009) *Toxicol. Appl. Pharmacol.* **238,** 221–239
50. Aisen, P., Leibman, A., and Zweier, J. (1978) *J. Biol. Chem.* **253,** 1930–1937
51. Perrin, D. D., and Watt, A. E. (1971) *Biochim. Biophys. Acta* **230,** 96–104
52. Andersen, O. (1984) *Environ. Health Perspect.* **54,** 249–266
53. Norden, A. G., Lapsley, M., Lee, P. J., Pusey, C. D., Scheinman, S. J., Tam, F. W., Thakker, R. V., Unwin, R. J., and Wrong, O. (2001) *Kidney Int.* **60,** 1885–1892
54. Yang, J., Goetz, D., Li, J. Y., Wang, W., Mori, K., Setlik, D., Du, T., Erdjument-Bromage, H., Tempst, P., Strong, R., and Barasch, J. (2002) *Mol. Cell* **10,** 1045–1056
55. McGraw, T. E., Greenfield, L., and Maxfield, F. R. (1987) *J. Cell Biol.* **105,** 207–214
56. Ward, J. H., Kushner, J. P., and Kaplan, J. (1982) *Biochem. J.* **208,** 19–26
57. Tabuchi, M., Yoshimori, T., Yamaguchi, K., Yoshida, T., and Kishi, F. (2000) *J. Biol. Chem.* **275,** 22220–22228
58. Erfurt, C., Roussa, E., and Thévenod, F. (2003) *Am. J. Physiol. Cell Physiol.* **285,** C1367–C1376
59. Bremner, I. (1987) *Prog. Food Nutr. Sci.* **11,** 1–37
60. Flo, T. H., Smith, K. D., Sato, S., Rodriguez, D. J., Holmes, M. A., Strong, R. K., Akira, S., and Aderem, A. (2004) *Nature* **432,** 917–921
61. Viau, A., El Karoui, K., Laouari, D., Burtin, M., Nguyen, C., Mori, K., Pillebout, E., Berger, T., Mak, T. W., Knebelmann, B., Friedlander, G., Barasch, J., and Terzi, F. (2010) *J. Clin. Invest.* **120,** 4065–4076
62. Liu, Z., Yang, A., Wang, Z., Bunting, K. D., Davuluri, G., Green, M. R., and Devireddy, L. R. (2011) *J. Biol. Chem.* **286,** 20606–20614